Sādhanā Vol. 28, Parts 3 & 4, June/August 2003, pp. 739–761. © Printed in India

Study of engineering surfaces using laser-scattering techniques

C BABU RAO and BALDEV RAJ

Indira Gandhi Centre for Atomic Research, Kalpakkam 603 102, India
e-mail: dmg@igcar.ernet.in

Abstract. Surface roughness parameters are described. Various surface characterization techniques are reviewed briefly. Interaction of light with the surface is discussed. Laser-scattering methods to characterise the surface are detailed. Practical cases, where laser-scattering methods have provided useful information about surface characteristics, are illustrated.

Keywords. Roughness; profilers; corrosion; scattering; specular reflection.

1. Surface roughness–An introduction

Roughness is a universal characteristic of all surfaces, and can take many forms (Bennett 1992a). In machined components, it often consists of minute scratches in random directions that remain after polishing or of grooved structures produced by turning or any other machining process. Grain relief on a polished metal mirror, distinct random machining marks left on a finished metal or fine parallel grooves on a glass surface that has been precision-ground are some of the features that characterise a surface. Scratches or pits are sometimes caused by improper handling. Some materials such as ceramics or silicon carbide contain voids, while others including aluminum or beryllium have hard inclusions in their bulk; all these things can appear on the surface. Optical or magnetic films applied to surfaces can add their own characteristics. Optical dielectric films such as silicon dioxide, titanium dioxide, zinc sulphide and magnesium fluoride are generally extremely smooth and contour the surfaces on to which they are deposited. Silver, gold, and copper films, in particular, tend to be slightly lumpy, adding additional fractions of nanometre roughness to the surface of the substrate. Metal films such as aluminum, platinum, nickel, and rhodium are smoother when there are fine grained. Magnetic films applied to aluminum or plastic surfaces and used to store information in dense arrays are generally quite rough compared to optical films. Optically black materials that absorb and/or scatter light are even rougher. These coatings have steep slopes and contain tiny holes acting as light traps because of multiple scattering.

Fingerprints, dust and other particulates, surface contamination in the form of pollutants in the air, or oil films, which loosely adhere to the surface are not part of surface roughness. In principle, these features can be removed from surfaces. However, in practice it may be difficult or even impossible to remove them without damaging the surface. In particular, thin film coatings may complicate the removal of unwanted surface contamination. Surface

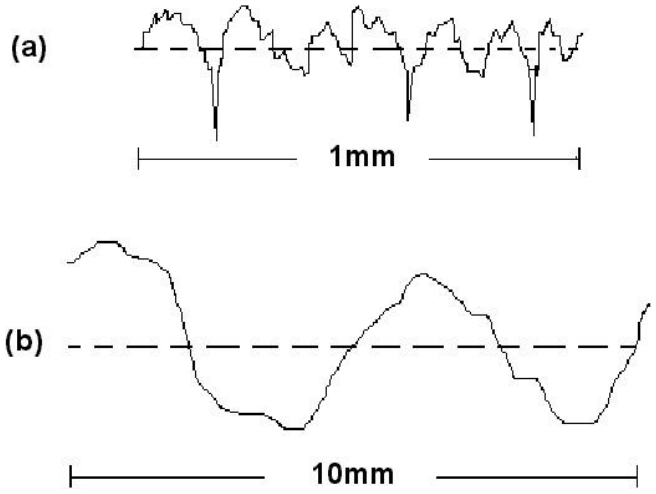

Figure 1. Profiles of different surface features: **(a)** polishing marks, grains structure, scratches, **(b)** waviness (vertical scale is magnified 1000 times as compared to the horizontal scale).

contamination may not be significant for mechanical components, but is of utmost concern on certain surfaces like semiconductor wafers and high quality optical elements. Thus cleanliness levels, commensurate with performance and end-use, are of paramount importance while manufacturing and processing surfaces.

Surface roughness has two main attributes: roughness heights (or depths) and lateral dimensions. Figure 1 shows profiles of (a) polishing marks, grain structure, and scratches, and (b) waviness. Scratches are a few tenths of a micrometre deep and a few micrometres wide, whereas waviness is of the order of millimetres.

Roughness heights of the structure on polished or machined surfaces are frequently measured and reported as the root-mean-square of roughness, σ. The units are ångstroms or nanometres for smoother surfaces and micrometres for rougher surfaces. Lateral dimensions, frequently called surface spatial wavelengths, are measured in micrometres.

Surface structure can be classified into three general groups according to its lateral dimensions. Surface microroughness (often called roughness) has lengths in the range of nanometres to one millimetre and includes thin films, polishing marks, scratches and grain structure. Surface waviness, or mid-spatial-frequency roughness, has lengths from a few millimetres to perhaps one centimetre. Chemically polished surfaces on silicon wafers exhibit mid-spatial-frequency roughness. The overall surface shape, often called the optical figure (departure from a perfect surface of the desired shape) or form in the machining industry, has lengths in the centimetre range to the size of the piece. Some objects such as tiny lenses or microspecimens are smaller than a centimetre. Their optical figure and waviness overlap.

This paper primarily focusses on roughness rather than waviness or optical figure.

2. Description of the rough surface

No two rough surfaces are identical. Even those formed by well-controlled processes, such as turning, each possess a unique surface form. In surfaces created under less controlled process conditions, such as sand-blasted surfaces or fracture surfaces, the random nature is even more apparent.

A rough surface is usually described in terms of its deviation from a smooth reference surface. The root mean square (RMS) height of the surface is given by

$$\sigma = \langle h^2 \rangle_S^{1/2}, \tag{1}$$

where h is deviation in height from a smooth plane.

3. Surface characterisation techniques

3.1 *Imaging methods*

Microscopes ranging from optical microscopes, scanning electron microscopes and transmission electron microscopes to scanning probe microscopes can obtain images of surfaces. These latter instruments can be used to produce topographic maps of surfaces on an atomic scale, both laterally and vertically (Wickramasinghe 1989; Pool 1990).

A scanning tunneling microscope (STM) can be used to produce a topographic map of the electron density, if the surface is conducting. The STM has an exceedingly sharp metal probe (of the order of atomic dimensions) that almost touches the surface. A small tunneling current flows between the probe and the surface. As the probe or surface is moved, the tunneling current changes as the probe-surface separation distance changes. A sensitive servo system moves the probe in the vertical direction to keep the tunneling current constant. This vertical distance that the probe moves, as a function of spatial location on the surface, is used to make a map of the conducting surface. This is assumed to be the same as the topographic surface.

Some surfaces are non-conducting. Maps and profiles of the surface topography of such surfaces can be obtained by using atomic force miscroscopy (AFM), This works on a principle similar to that of STM. Here a sharp but non-conducting probe contacts the surface. The deflection of the cantilever holding the probe is measured. As the surface height changes, the cantilever deflection changes. The amount of vertical motion needed to restore the cantilever deflection to its original value is plotted as a function of spatial location on the surface.

In the scanning electron microscope (SEM), electrons are scattered from the surface of the specimen and strike a collector which generates an electrical signal. This signal is subsequently processed and used to form an image representing the specimen surface on a monitor screen. Conductive specimens can be inspected directly. For large specimens, replicas have to be taken for inspection. In SEM, the specimen has to be inclined while imaging. The surface topograph manifests as a shadow image. Appropriate slopes are required to produce images with good contrast.

Several special problems arise when examining specimens with electron microscopy. First, specimens must be small in order to fit into the specimen cell of the microscope. As a result, the examination of the surfaces of large components can only be achieved by destructive means, i.e. cutting the specimen, or by taking replicas which may be unreliable. Specimens must preferably be electrically conductive. However, non-conductors can be examined successfully by coating them with a thin layer of metal by a vacuum evaporation process. The examination of surfaces using electron microscopy is never a quick operation. The preparation of the specimen takes some time as does the formation of the vacuum in the microscope, which is required so that electrons can travel through the microscope without being scattered by air molecules. The interpretation of the images it forms is not necessarily straightforward and they do not readily yield quantitative data about the height of surface features. Much effort and great expertise are required to show shallow structures like a diamond-turned metal surface

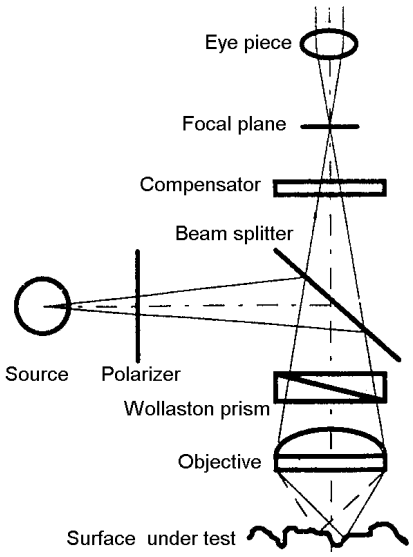

Figure 2. Schematic diagram of Nomarski microscope.

(Bennett 1992b). In spite of all this, electron microscopy is a popular technique used in the investigation of surface structures and wear particles (Sherrington & Smith 1988).

A differential interference contrast microscope or Nomarski microscope (Lessor *et al* 1979; Bennett & Mattsson 1989) is very frequently used for observing roughness structure. This instrument accentuates surface slopes. Two beams of light laterally sheared from a single beam strike the surface being inspected. Any surface features that produce phase differences between the two beams reflected by the surface become visible as shades of gray illuminating the surface features. Lower magnifications are generally preferable because surface slopes are larger and the contrast in the image is better. A typical Nomarski microscope is shown in figure 2.

Confocal microscopy is another alternative for producing topographic maps of surfaces whose roughness heights are large compared with the focal range (depth of focus) of a microscope objective, i.e. $> 1\,\mu$m (Hamilton & Wilson 1982; Wilson *et al* 1986; Matthews *et al* 1986; Sheppard & Matthews 1988). A tiny area on a surface is imaged on a detector masked by a pinhole. If the area is in focus, the detector has maximum signal output. If the area is out of focus, the detector signal is lower. Two options are possible: (a) move the imaging lens and detector until the signal is maximized and note the distance the lens has moved, or (b) calibrate the reduced signal level to correspond to the amount of defocus of the surface.

Ogilvie *et al* (2001) have used high fidility polymer models (HFPMs) (replicas) made from transparent epoxy and accurate to within $1\,\mu$m, for obtaining the topography of fractured surfaces. The method relies on the calibration of transmission of a dyed fluid with accurately known thickness. This calibration obeys the Lambert–Beer law. The HFPM (replica) of the fracture surface is covered with dyed fluid. The transmission image of the dyed fluid gives the thickness of the fluid trapped in the HFPM. This essentially gives the topography of the rough surface from which the replica is taken.

A word of caution is appropriate while discussing imaging methods. These measurements are dependent on many factors like surface chemistry, microstructure etc., in addition to the topography of the surface. Therefore one has to choose the method appropriately and interpret the results judiciously.

3.2 *Comparative methods*

Comparative devices are relatively inexpensive, they are quick to apply and they do not require extensive special training to operate. The most well-known comparative measurement technique is the finger-nail test. Here, the finger/finger nail is drawn across a specimen. The "feel" (i.e. the frictional resistance) of the specimen is compared with that of a set of calibrated samples manufactured by the same process. The sample whose "feel" most closely resembles that of the specimen is noted. The tactile test is more reliable than simple visual inspection as a method for assessing surface roughness. However, this does not provide a quantitative measure. The technique is more sensitive to the range of surface roughness rather than average roughness (Church 1979). Rubert describes an instrument which attempts to simulate tactile comparison, to eliminate the subjective element of human judgement (Thwaite 1980b).

Some comparative methods involve capacitance measurement (Sherwood & Crookall 1968; Brecker *et al* 1977), and inductance measurement (Radhakrishnan 1977). The pneumatic method (air gauging) measures the flow of air through a gap between a specimen surface and an open-ended nozzle placed face-down on it and correlates the gap with the surface roughness (Graneck & Wunsch 1952; Wagner 1967; Radhakrishnan & Sagar 1970; Tanner 1979).

3.3 *Profiling methods*

Both mechanical and optical profilers are used to take profiles of the surface along a line or make topographic maps of an area. A good review of commercial systems is given by Bennett & Mattsson (1989).

A common-form of mechanical profiler comprises a stylus transducer (Bennett & Dancy 1981). This employs a linear variable differential transformer (LVDT), figure 3. A beam, pivoted on two knife edges, carries the stylus at one end and a ferrite block at the other. The ferrite block is located between two coils. As the stylus is drawn over the irregularities of a surface by the traverse unit, the stylus is displaced, causing the ferrite rod to move between the coils. The coils form part of an inductance bridge circuit which is balanced when the stylus is in a neutral position. When the stylus changes position, it causes a change in the mutual inductance in the coils modulating a high-frequency carrier signal in proportion to the displacement of the stylus. The relative change in the phase of the carrier signal indicates the direction of displacement of the stylus. The carrier signal is amplified and de-modulated to yield a signal representing

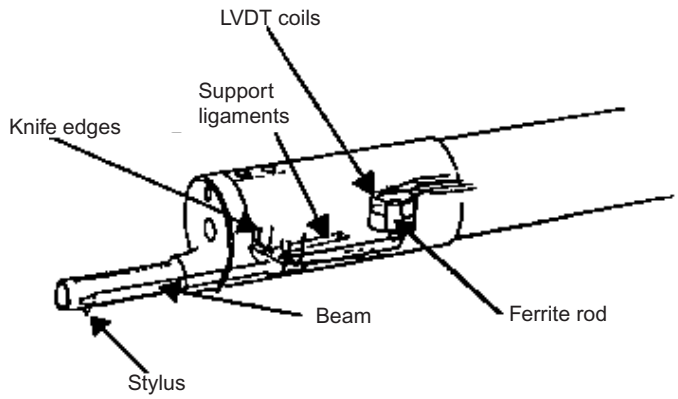

Figure 3. Stylus probe of mechanical profilometer.

a surface profile which may be output to a chart recorder or used to evaluate some parametric assessment of surface roughness given on a metre or visible display unit. In addition to LVDTs, several other forms of displacement transducers are in use, e.g. optical interferometers, variable capacitors. A comprehensive review of transducer design is given by Garatt (1979). The height sensitivities of the most sensitive mechanical profilers are in the subnanometre range.

The Chapman microprofiler is a typical optical profilometer (Bristow *et al* 1988). It uses two light beams of orthogonal polarizations, focused on the surface, produced from a single beam by a laterally shearing Wollaston prism. These beams, a micrometre or so in diameter and separated by a distance approximately equal to the beam diameter, sense surface height differences that produce deviations in the reflected beam intensities. Two detectors, one for each beam, measure these variations. These data are reduced to give the slope of the surface. The output is integrated once to yield a surface profile. The height sensitivities of the optical profilometers are in the subnanometre range.

There are many other types of optical and mechanical profilers described in the literature (Bennett & Mattsson 1989; Bennett 1992a). Mechanical profilers have better lateral resolution, a larger height measurement range, frequently up to many micrometres, and are not affected by the material (optical constants or transparency) of the surface as long as it is not too soft. On the other hand, because the diamond stylus contacts the surface, it can leave a track unless the loading is very carefully controlled. Despite some disadvantages, mechanical profiler has proved versatile and reliable in both the manufacturing and the research environment. For many years, the most popular device used to measure surface topography has been the stylus instrument. It is also the instrument by which many standards are defined (Sherrington & Smith 1988).

The obvious advantage of any optical profiler is that, since it is non-contact, it cannot damage the surface. The main disadvantages of the optical profilers are: (a) their lateral resolutions are limited by the properties of the optical systems and by the light beams illuminating the surfaces, (b) these are sensitive to the phase of the light reflected from the surface, and cannot distinguish between changes in topography and changes in optical constants of the surface, and (c) the maximum step height that can be measured is less than half of the incident wavelength. The 1–2 μm lateral resolution is not sufficient to resolve normal fine scratches and other surface details. As a consequence, roughness values obtained using optical profilers tend to be smaller than those measured with contact probe-type instruments on the same surfaces (Bennett 1992b).

We discuss, in the following, optical scattering methods, after discussing the interaction of light with rough surfaces.

4. Interaction of light with a rough surface

When light is incident on a rough surface, it may be reflected specularly, diffusely or both. The proportion of diffuse to specular reflection depends on the relation between the roughness of the surface and the wavelength of the incident radiation.

Consider a plane monochromatic wave incident at some angle θ_i onto a rough surface (figure 4). For waves scattered into the XZ plane at some angle θ_S, the phase difference between two rays scattered from separate points X_1 and X_2 on the surface is given by

$$\Delta\phi = k[(h_1 - h_2)(\cos\theta_i + \cos\theta_S) + (X_2 - X_1)(\sin\theta_i - sin\theta_S)], \tag{2}$$

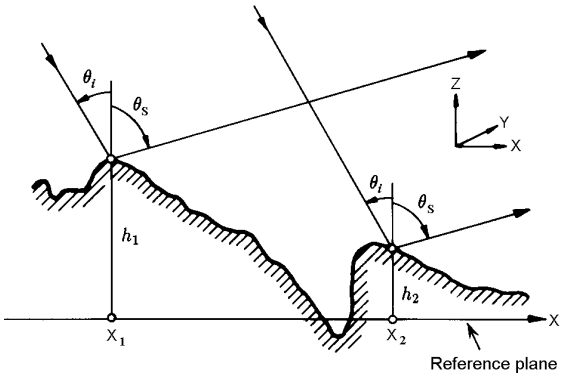

Figure 4. Schematic illustrating the phase difference between two parallel rays scattered from different points on a rough surface.

where k is the modulus of **k**, the incident (and scattered) wavevector ($k = 2\pi/\lambda$). The heights of these points, from some reference plane, are h_1 and h_2.

For a smooth surface, where $h_1 = h_2$ everywhere, the phase difference becomes

$$\Delta\phi = k(X_2 - X_1)(\sin\theta_i - \sin\theta_S). \tag{3}$$

In the specular direction, $\Delta\phi = 0$ for all sources across the surface, and wavelets constructively interfere to give the strong specularly scattered field. This is modified for smooth surfaces of finite extent, where strong scattering occurs in, and around, the specular direction, with the width of this *lobe* of energy dependent on the dimensions of the surface relative to the incident wavelength.

If a surface is such that generally $h_1 \neq h_2$, then the surface may scatter radiation as though it is rough. Then destructive interference occurs in the specular direction, reducing the amplitude of the specular field. The extent to which this is reduced is dependent on the average value of $\Delta\phi$ across the surface. This reduction may be approximated by $\exp(-g/2)$ where for specular scattering or backscattering is given by (Beckmann & Spizzichino 1963),

$$g = 4k^2\sigma^2\cos^2\theta_i. \tag{4}$$

The parameter g is a measure of the roughness of a surface, representing the mean square phase variations undergone by a wave when scattered from many points across the surface.

For non-specular scattering from a rough surface, i.e. away from the specular reflection, the phase in any direction is determined by the height variations across the surface. This scattered energy is usually termed the diffuse or *incoherent* field, because of its wide angular spread and lack of phase relationship with the incident wave. Similarly, the specular wave is often termed the *coherent* field, due to its predictable, and constant, phase relative to that of the incident wave. Figure 5 depicts, schematically, the expected change in energy distribution scattered from surfaces of increasing roughness.

5. Laser-scattering parameters

Based on the concepts discussed above, many methods have been proposed to evaluate the surface roughness (Vorburger & Teague 1981; Sherrington & Smith 1988; Bennett 1992b). For a recent review of works using laser-scattering techniques one can also refer to *Proc. SPIE* (2000).

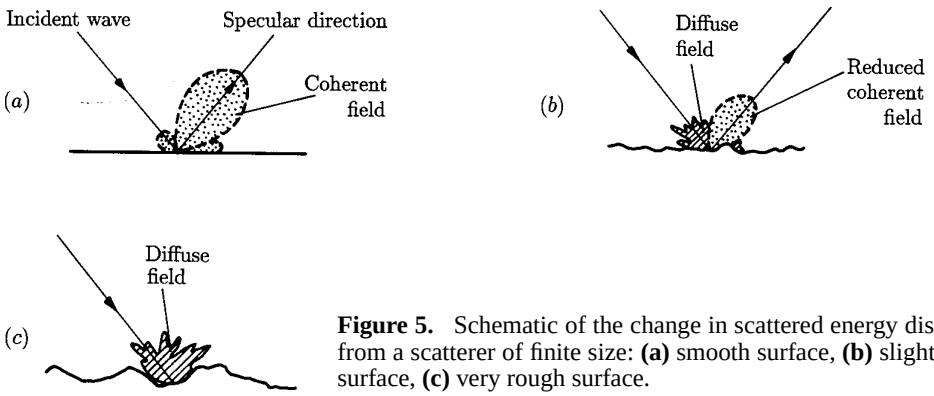

Figure 5. Schematic of the change in scattered energy distribution from a scatterer of finite size: **(a)** smooth surface, **(b)** slightly rough surface, **(c)** very rough surface.

5.1 *Specular component*

Beckmann & Spizzichino (1963) have shown that if σ is much less than λ and the surface has a Gaussian height distribution, the intensity of the specular beam is given by

$$I_{SP} = I_0 \exp\left\{-(4\pi\sigma\cos\theta/\lambda)^2\right\}, \tag{5}$$

where θ is the angle of the incident ray and I_0 is the total reflectance of the rough surface. (I_0 is found by measuring the total light intensity scattered into all directions, including the specular light.) Equation (5) permits σ to be derived from measurements of I_{SP}, the specular beam intensity.

5.2 *Scattered component*

As surface roughness increases, the pattern of the scattered radiation tends to become more diffuse. Measuring the total intensity of diffusely scattered light, a technique known as the "total integrated scatter" (TIS) method has been used to assess the roughness of surfaces with an σ of up to 0·01 μm. The technique is complementary to specular reflectance measurements. If light of wavelength λ illuminates a surface with a Gaussian height distribution, then using (5)

$$TIS = 1 - \frac{I_{SP}}{I_0} = 1 - \exp\left\{-\left(\frac{4\pi\sigma\cos\theta}{\lambda}\right)^2\right\} \approx \left(\frac{4\pi\sigma\cos\theta}{\lambda}\right)^2. \tag{6}$$

This allows σ to be calculated from scatter intensity measurements.

Bennett (1978) describes a TIS measurement system (figure 6). An aluminized collecting sphere, called a Coblentz sphere, focuses diffusely scattered light on to a detector D_1. A

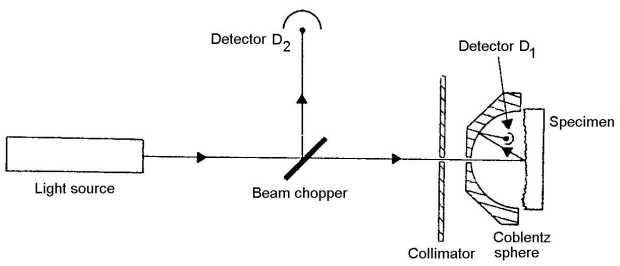

Figure 6. Schematic diagram of TIS measurement sytem.

"chopper" mirror throws incident light into a second detector D_2 and the specimen in alternation. The quantities I_{SP} and I_0, required for a roughness measurement, can thus be estimated from the detector signals.

5.3 *Angular distribution of scattered light*

Using scalar scattering theory, it can be shown that the angular distribution of light scattered from a rough surface directly maps the power spectral density $P(K)$ of the surface topography (Church 1979). For light normally incident on a specimen surface, it has been reported that the scattering angle θ_S, is related to the roughness component. The angular distribution of the scattered radiation $I_S(\theta_S)$ is related to the power spectrum (Sherrington & Smith 1988),

$$I_S(\theta_S) = \lambda^{-4} r(\theta_S) P(K), \tag{7}$$

where $r(\theta_S)$ is a geometric factor which depends on the scattering angle. The advantage of angular distribution measurements over other forms of scatter measurement is that they supply spatial data as well as height information about surface roughness. Several investigators have constructed angular scattering measurement systems to measure the roughness of optical components and other "high finish" surfaces (Church 1979; Thwaite 1980a; Hingle & Rakels 1983; Rakels 1986; Cao *et al* 1991).

5.4 *Dual parameter approach*

A dual parameter approach is adopted at the authors' laboratory. The experimental setup used in these studies essentially comprises a laser source, beam steering optics, specimen holder and an intensity measuring device. Two intensity-measuring devices are used in this study. When the scattering pattern exhibits symmety, a linear scanner is used. A photodiode mounted on a mechanical scanner is used for measuring the intensity. The schematic diagram of the optical configuration using linear scanner is shown in figure 7. When there is asymmetry expected in the scattering pattern, the linear scanner is replaced by a CCD camera to acquire the image of the scattering pattern. A cooled camera with a 16-bit dynamic range is used for this purpose. The two-dimensional intensity distribution in this image is used to understand the scattering pattern.

Various parameters that can be used in characterising the scattering pattern have been discussed in previous sections. For smooth surfaces, when the RMS roughness σ is less than the wavelength of light (λ), most of the radiation is specularly reflected at an angle

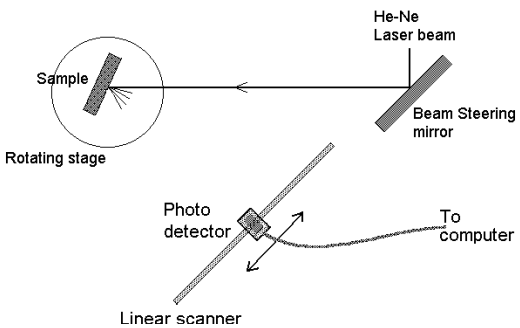

Figure 7. Schematic diagram of the laser-scattering set-up using linear scanner.

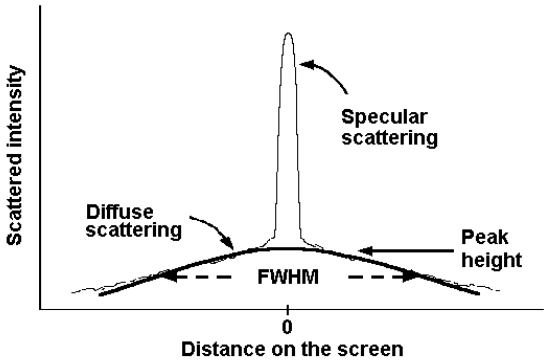

Figure 8. Typical scattering pattern consisting of specular reflection and diffuse scattering. The position marked '0' on the distance on the screen axis corresponds to the angle of reflection.

equal to the angle of incidence (figure 8). As the roughness increases, scattering becomes more diffuse. In order to cover better range of roughness, both these parameters are considered to understand the surface characteristics. The intensity of the specular reflection is adopted as one of the parameters (Stout 1984; Whitley *et al* 1987). The intensity across the diffuse scattering pattern is scanned and the full width at half maximum (FWHM) of the diffusive scattering pattern is taken as the second parameter (Clarke & Thomas 1979).

The intensity (I) collected with the linear scanner is normalised with respect to the intensity (I_0) of the specular reflection from a polished surface of the same material as that of the specimen, with the same optical set-up as that used for the specimen. The background intensity is subtracted from each of the normalised data (I/I_0). The specular reflection is measured in arbitrary units.

The specular reflection can be identified without difficulty for smooth surfaces with $\sigma < \lambda$. It is characterised by an intense peak distinct from the diffuse scattering pattern. The intensity along the angle of reflection can easily be measured. However, it becomes difficult to measure specular reflection from surfaces with $\sigma > \lambda$. The second parameter is useful in this domain of roughness. The component due to diffuse scattering is fitted to a Gaussian curve (figure 8). Peak height (PH) of the diffuse scattering is estimated from this curve. FWHM is the width of the scattering at half this PH. The FWHM is measured in millimetres.

6. Specific cases

We now briefly discuss a few examples where laser-scattering studies have given useful information about the surface based on roughness measurement.

6.1 *Scattering from ground surfaces*

Figure 9 shows the laser-scattering pattern from ground rough surface standards (Rugotest 104 ground surfaces, wavelength of the laser used He–Ne $\lambda = 0{\cdot}63\,\mu$m). The angle of incidence of the beam is kept at 45°. The beam width on the surface is about 1 mm in diameter. The intensity of the specular reflection, I/I_0, measured on these patterns is shown as a function of logarithm of roughness of the scattering surface in figure 10. There is a good linear relationship up to a roughness of about $0{\cdot}8\,\mu$m. Beyond this value of roughness, specular reflection is not a reliable parameter.

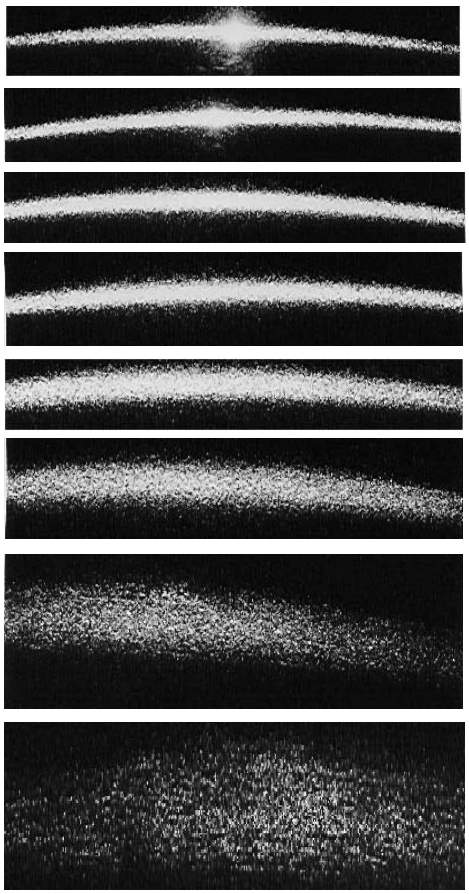

Figure 9. Laser-scattering pattern from ground surface standards.

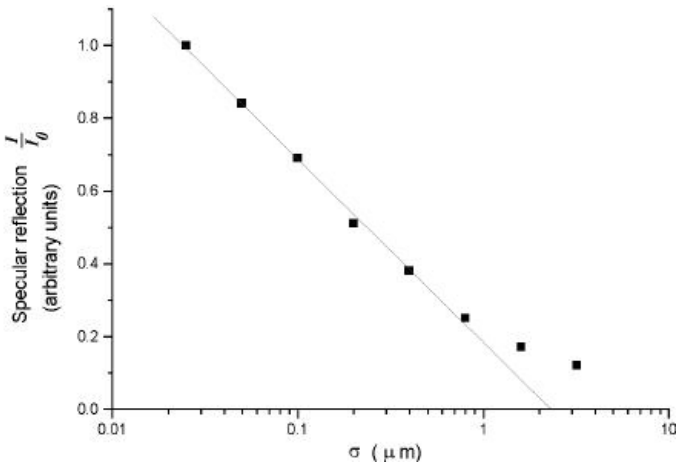

Figure 10. Specular reflection as a function of RMS roughness σ.

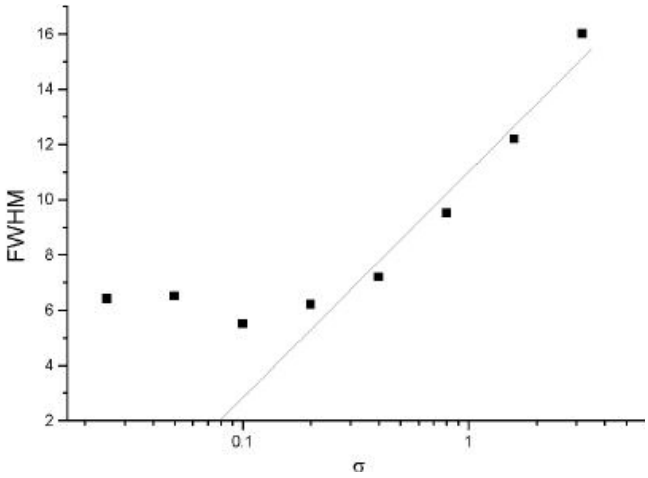

Figure 11. Full width at half maximum (FWHM) as a function of RMS roughness σ, FWHM is measured across the scattering pattern (i.e. in the vertical direction in figure 9).

It may be noted that the spread of the scattering pattern is perpendicular to the lay of the grinding marks. The RMS roughness is measured perpendicular to the lay. Therefore, in principle, FWHM measured along the scattering pattern gives a measure of the RMS roughness. Since the scattering is spread into a wide angle, and since scattering is conical due to 45° angle of incidence, the measurement of FWHM along the scattering pattern (i.e. along the horizontal direction in figure 9) is difficult. The intensity distribution across the scattering pattern (i.e. along the vertical direction in figure 9) is measured to investigate whether this would suffice. Figure 11 gives FWHM, thus measured on the scattering patterns as a function of logarithm of roughness of the scattering surface. There is good linear relationship in the roughness range from 0·2 μm up to 3·2 μm. The measurement of FWHM is unreliable in the scattering pattern from very smooth surfaces, with RMS roughness σ less than the wavelength of the laser λ.

This FWHM measured across the scattering pattern gives a measure of the roughness along the lay, i.e. along the surface of the grinding marks. The study indicates that there is good relationship between this measure and the RMS roughness measured perpendicular to the lay. This may be so because the shearing of the material by the grinding tool leaves a coarse surface along the grinding mark for larger σ, and a smoother surface for lower σ.

6.2 *Scattering from machined surfaces*

In general, most of the work on laser-scattering from machined surfaces, understandably, is oriented to provide alternatives to stylus profilomcters, which has resulted in quite a few practical instruments. It is mainly aimed at rendering measurement results that agree with the profilometer results, with which industry is familiar. Although this is a prerequisite, one should also look into the possibility of utilising the additional advantages that the optical techniques might provide. The laser beam (probe) after interacting with the surface carries detailed information about the surface topography also. In order to extract this information, one should have clear understanding of the light-scattering behaviour from surfaces. The theory of light scattering from *random surfaces* is well understood. However, despite the large amount of research effort, the general scattering problem has yet to be solved, and there are many engineering processes, each leading to a distinct surface texture. Often, this texture is unisotropic. Detailed surface characterisation plays an important role not only in providing

information about the surface finish, but also a possible feedback on tool shape, machine tool condition, machine bed vibrations. Enough work is not done in this direction. This calls for detailed studies on light-scattering behaviour from each of the machined surfaces, obtained from a variety of engineering processes.

A turned surface standard (JIS •) has been considered for this study. It is a cylindrical surface with turned grooves at regular pitch. Though the surface is cylindrical in shape, the standard contains only the representative sections. It contains six standard surfaces each with a different pitch. These are designated as SN-5 to SN-10. The remaining six surfaces are coarse surfaces or ground surfaces, which were not considered in this study. The typical pitch of the grooves is approximately 80, 150, 300 and 600 μm, for SN-7 to SN-10. The pitch angle η, measured with a profiling microscope, is 157°. The pitch is approximately 20 μm and 40 μm for SN-5 and SN-6 respectively. The pitch angle η could not be measured for these two surfaces, since focusing on to the edge was difficult. All the surfaces of this standard are fairly reflective. The σ of the surfaces SN-5, SN-6, SN-7, SN-8, SN-9 and SN-10 are 1·6, 3·2, 6·3, 12·5, 25, and 50 μm respectively (marked on the surface standard and certified in its technical brochure).

Figure 12 shows the typical scattering patterns from turned surface standards (SN-5 to SN-10), when the laser beam is incident perpendicular to the surface. Two similar scattering patterns are formed on either side of the beam, designated as **L** (left) and **R** (right) patterns. The angular separation between the **L** and the **R** patterns (46° in this case) is characteristic of the machined groove, which in turn is a function of the machine tool used. The diffraction phenomenon is less distinct and specular scattering from the surface of the grooves is more predominant for grooves with a larger pitch (starting from SN-10). As the pitch of the grooves decreases, the diffraction phenomenon becomes more distinct. Since the surface is cylindrical, each diffraction fringe thus formed is elongated and extended into an arc. Clearly, these scattering patterns offer a scientific way of qualitatively differentiating the machined surfaces compared to the finger-nail test. By analysing the intensity distribution, one can study the surface profile of the machined groove. This can provide valuable information about the machining conditions and the tool tip.

Another important aspect in the machined surfaces is periodic error in the grooves. The fine pitched grooves give rise to diffraction in the laser-scattering pattern. Periodic errors introduce satellite peaks, apart from the diffraction peaks due to machined grooves. The spacing of the satellite peaks depends on the periodicity of the error, and amplitudes depend on the amplitude of this periodic component. In practice, the periodic error is not a single component. It consists of a spectrum of periodic components. Correspondingly, the pattern shows satellite peaks (figure 13).

6.3 *Corrosion monitoring*

Corrosion is an important manifestation which affects the reliable operation of many component (Pearce 1997). Corrosion is essentially a surface phenomena. Thus optical methods offer the possibility to detect and monitor corrosion at an early stage. A few researchers have used various optical techniques for studying corrosion. The change in the density of the solution at the electrode causes a shift in the interference fringes. Chmiel *et al* (1990) have used

---

•JIS:Japanese Institute of Standards (JIS B0658*) — With machined surfaces, due to their random nature, it is difficult to reproduce specific observations/results. Surface standards guarantee a specific surface finish. This will ensure that the specific observations can be reproduced by other researchers as well.

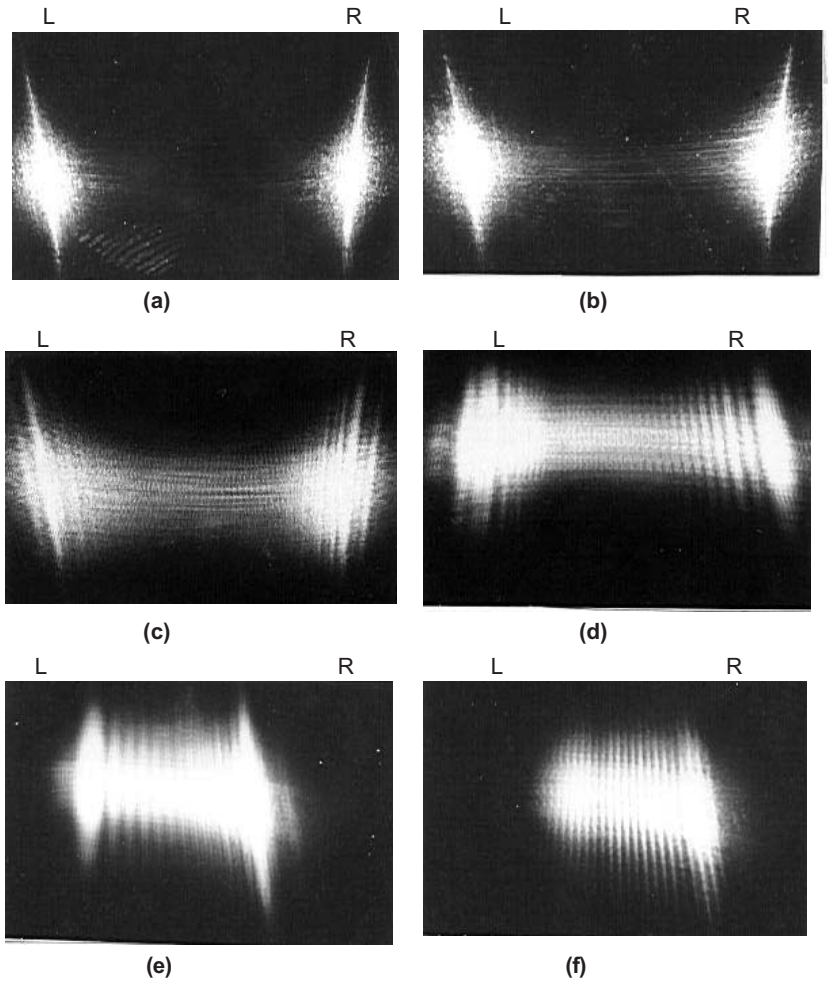

Figure 12. Typical scattering patterns from various surfaces of the turned surface standard JIS B0683 – with laser beam incident normal to the surface: **(a)** SN-10 (600 μm pitch), **(b)** SN-9 (300 μm pitch), **(c)** SN-8 (150 μm pitch), **(d)** SN-7 (80 μm pitch), **(e)** SN-6 (40 μm pitch), **(f)** SN-5 (20 μm pitch).

optical interferometry to measure this shift and study corrosion. Escalona *et al* (1993) have used phase shifting interference microscopy for the analysis of corrosion pitting in 304 stainless steel with and without molybdenum ion implantation. Feng & Chiang (1997) have used digital speckle correlation technique for revealing pitting corrosion. Cluster of pits of 0·3 mm diameter and 0·1 mm depth are detected by this technique. Laser-scattering parameters have been correlated with sodium exposure of AISI type SS 316 surfaces (Vaidehi *et al* 1995). Anantha Lakshmi *et al* (1999) have studied pitting corrosion in AISI type 316 stainless steel specimens using laser-scattering parameters.

The objective of this study is to explore the correlation between laser-scattering parameters and intergranular corrosion (IGC). IGC is introduced in sensitised and polished AISI type 316 stainless steel specimens by electrolytic etching, Different extents of corrosion are obtained with different etching times. Since the scattering pattern is asymmetric in some cases, the

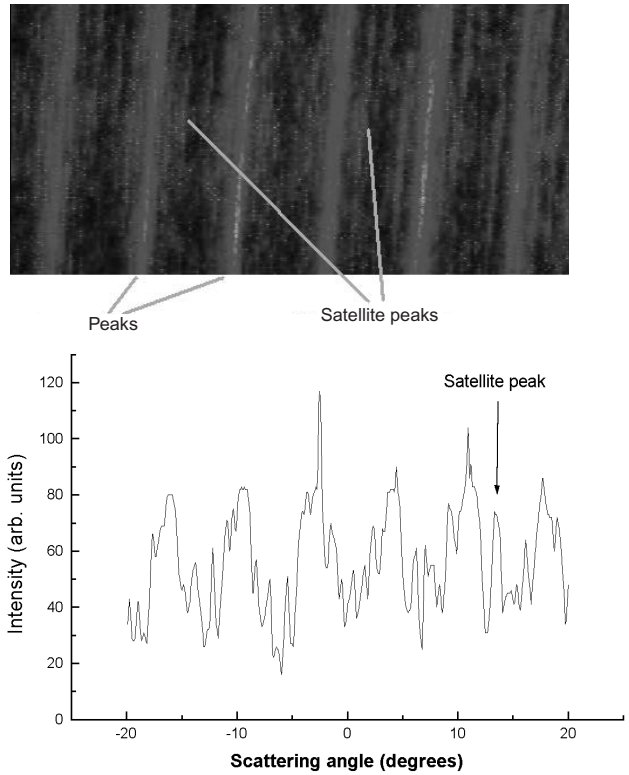

Figure 13. **(a)** Scattering pattern from a turned surface, showing satellite peaks, **(b)** corresponding intensity distribution.

scattered intensity distribution is recorded using the CCD camera. The image of the scattering pattern is smoothened and filtered to remove specular noise. This image is used for further analysis.

Some of the smoothened intensity distributions are shown in figure 14 as a function of etching time. The intensity distribution of the scattering pattern is Gaussian in nature, for the as-polished surface and when etching time is small. But at higher etching times ($\geq$ 50 s), some asymmetry is observed in the scattering pattern. Particularly for 60 s and 70 s etching times, distinct lobes can be seen in the intensity surface. With an etching time of about 70 s, it is observed that the etching (corrosion) occurs uniformly all along the grain boundary making the etched region an imprint of grain boundaries (figure 15). Thus the non-uniform scattering is due to the anisotropy in the microstructure of the specimen.

The specular reflection from the specimen is normalised with respect to that of the as-polished specimens with the same optical set-up. Figure 16 shows specular reflection as a function of etching time. Specular reflection decreases as the etching duration increases and tends towards an asymptotic value.

Thus the correlation between the monotonous behaviour of the specular reflection and the severity of corrosion in these test specimens strongly indicates the feasibility of using laser-scattering for on-line monitoring of corrosion. Particularly in the initial stages of corrosion, laser-scattering parameters can be taken as a reliable quantitative measure. Since corrosion is material-specific, individual calibration data are to be obtained for each material. It is also evident that sensitivity and quantitative nature of the information far exceeds other mapping methods of corrosion.

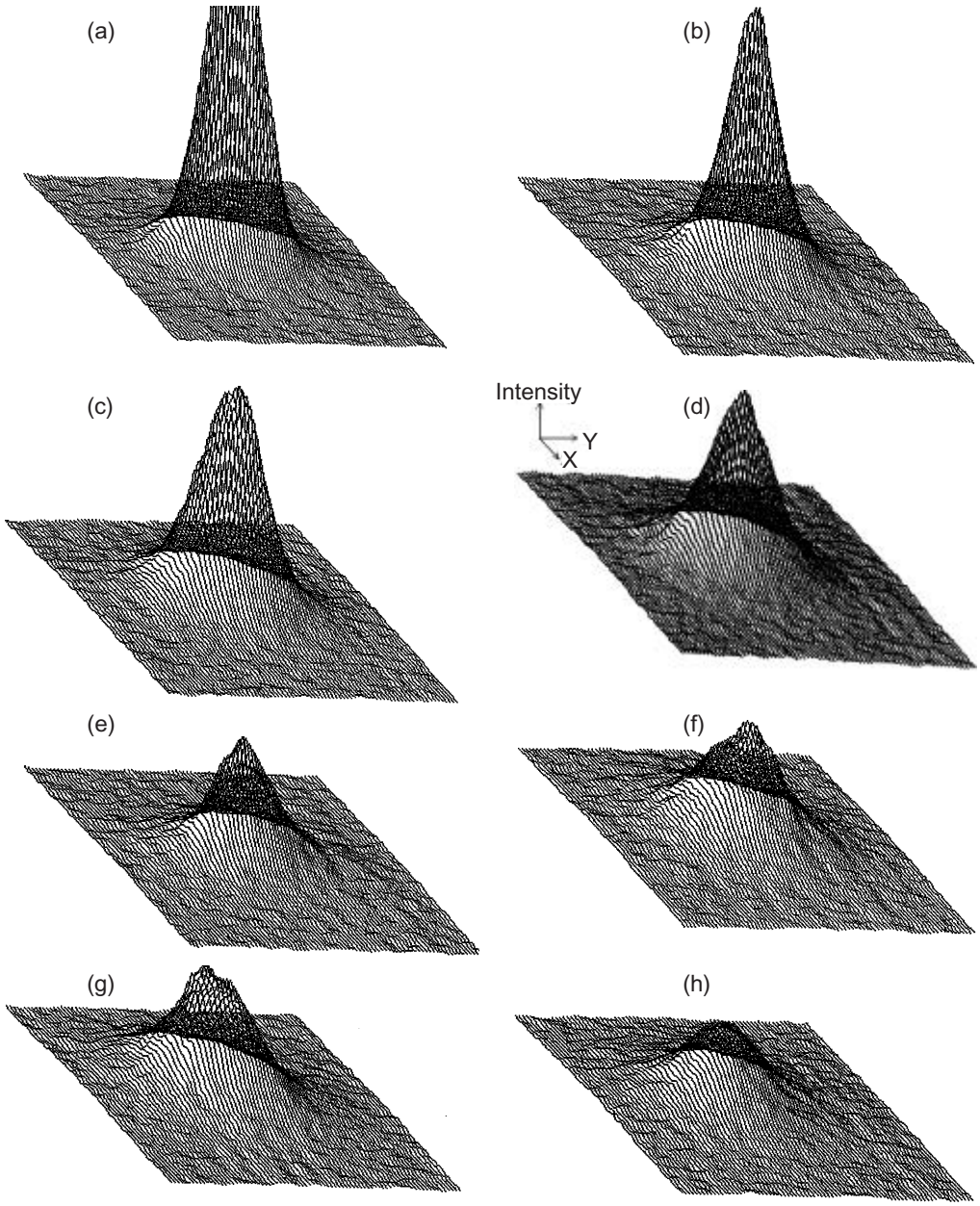

Figure 14. Intensity distribution of the scattering pattern, from the surfaces of the specimens with different etching times. The noise in the intensity distribution is removed using a Gaussian smoothening filter. **(a)** 0 s (as polished), **(b)** 20 s, **(c)** 30 s, **(d)** 40 s, **(e)** 50 s, **(f)** 60 s, **(g)** 70 s, **(h)** 80 s.

6.4 *Monitoring laser surface treatment*

Laser heat treatment using high power lasers is an important technology. Surface modification of metals and alloys using lasers is mostly employed to alter the surfaces for improving their

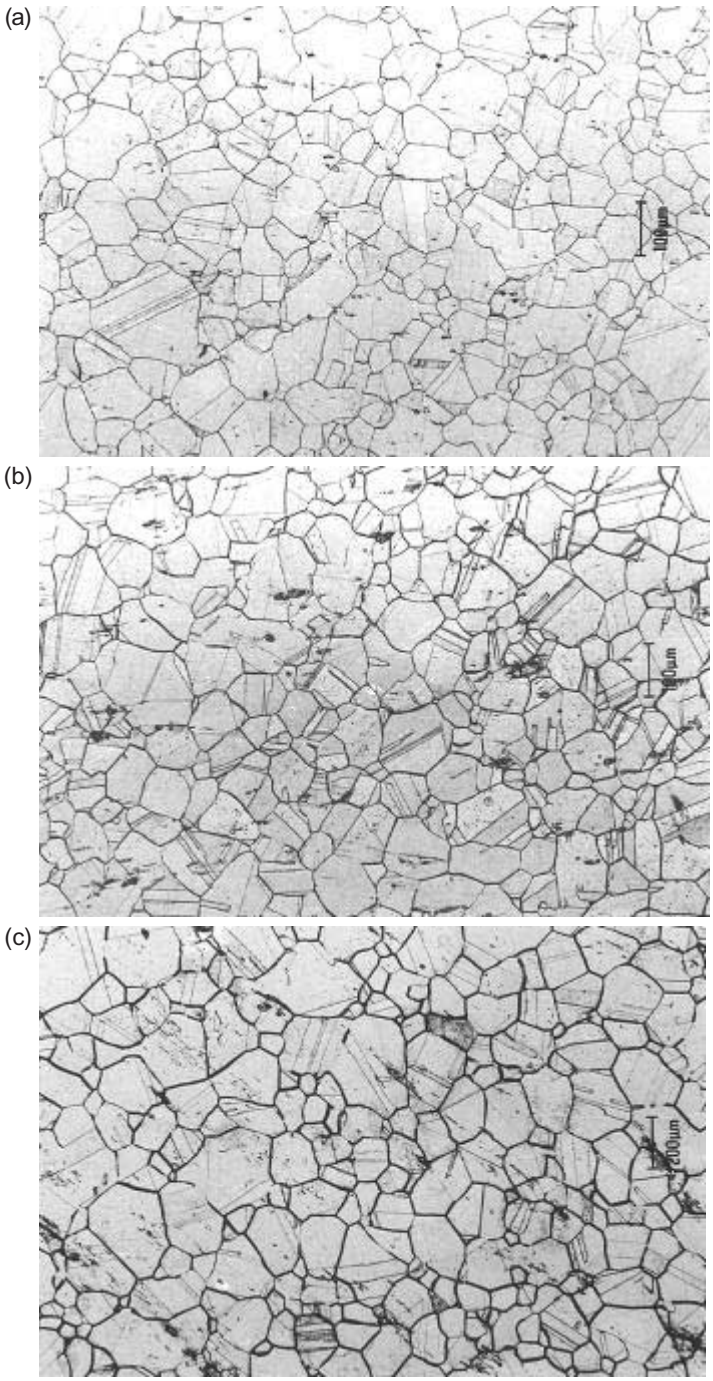

Figure 15. Micrographs of the etched surface with different etching times. Notice the erosion along the grain boundaries, which increases with increasing etching time. **(a)** 20 s, **(b)** 50 s, **(c)** 80 s.

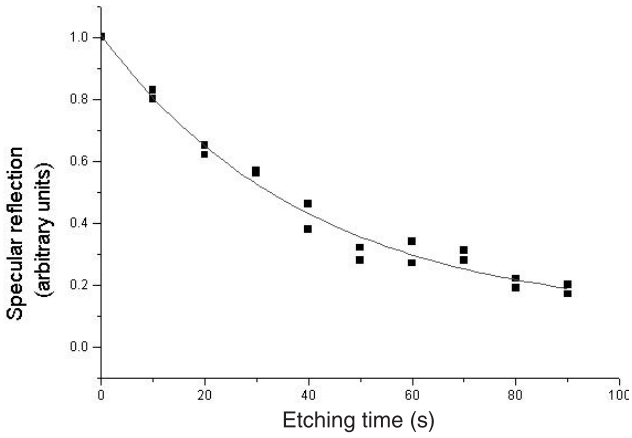

Figure 16. Specular reflection as a function of etching time.

mechanical properties such as hardness, wear resistance etc. (Pelletier *et al* 1993; Senthil Selvan *et al* 1999). The changes thus achieved are highly localised and confined to near-surface regions (10–100 μm depth). In this process the mechanical and structural properties of the bulk are retained as such. This is because of the high temperature gradient and high rate of change of temperature that are attainable by this method over an extremely localised region. Since laser heat treatment can be done in ambient conditions and also through fibre optic delivery, this process has an edge over the electron beam process. Transformation hardening is a typical process where laser heat treatment has distinct advantages. This is a process where hardening of the material is achieved by inducing phase transformations in the microstructure through heat treatment at suitable temperatures, normally below the melting point of the material. Conventionally, phase transformation can be induced by heat treatments, such as induction heat treatment, where the whole of the component is modified. In the laser surface modification process, a high power laser beam is used to heat a thin surface region rapidly, with the underlying bulk material providing self-quenching. By manipulating the laser power density and the time of interaction of the laser beam with the surface it is possible to achieve suitable microstructures with desired properties. Also by controlling the area/geometry of the region irradiated, the region of hardening can be localised.

In this context, there is a need to develop suitable techniques for quality evaluation. The laser irradiation parameters (power and the exposure) are to be controlled to ensure that melting does not occur. This calls for monitoring whether the surface irradiated is molten or not. Laser-scattering offers such possibility.

A continuous-wave CO_2 laser system (600 W operating at 10·6 μm) is used to irradiate the surfaces of polished stainless steel specimens. Each of them is polished to the same extent, up to 600 grit. Three different stages are observed which take place at different powers of the laser with different times of exposure. These three stages are surface browning, white hot without melting and initiation of melting. Table 1 gives the stages achieved with different powers and exposures.

For lower powers (50 to 100 W), no major changes are observed, even with long exposures, except faint browning of the surface. This implies the heat dissipation by the specimen compensates for the heat deposition by the laser beams. At powers of 150 W, the surface does not melt even with exposures of 240 s, except that the surface has reached white-hot condition. When power is raised to 200 W, surface melting is observed. However, even with the same

Table 1. Stages achieved with different powers and exposures.

Specimen No.	Power(W)	Exposure time(s)	Visual observation during irradiation
S-1	50	120	Surface browning
S-2	100	120	Surface browning
S-3	100	240	Surface browning
S-4	150	120	White hot – No melting
S-5	150	240	White hot – No melting
S-6	200	60	White hot – No melting
S-7	200	75	Melting initiated
S-8	200	120	Melting initiated
S-9	200	120	Melting initiated

power (200 W), melting is initiated with different exposures, in one case, within 75 s and in another case taking almost 60% more exposure time (120 s).

These results reveal the random nature of the relation between laser power and exposure parameters, and the energy absorption by the material. Although all the specimens are polished to the same extent of up to 600 grit, statistical variations might have influenced the absorption efficiency of the surface. Therefore the power of laser and the exposure needed to achieve the same stage is different for different specimens. This highlights the need for process monitoring apart from the laser parameters in order to ensure the desired surface modification. Our studies indicate that such process feedback is indeed possible by adopting laser-scattering techniques to monitor the surface. The laser-scattering pattern from these irradiated surfaces was obtained using CCD camera.

Since the specimens are polished up to 600 grit, the scattering pattern from a typical unirradiated polished surface shows predominant streaks perpendicular to the direction of polish (figure 17a). In some cases, more than one streak is observed. These streaks are distributed equally on either side of the central bright specularly reflected spot. The large extent of the scattering streaks over a wide angle essentially indicates high spatial frequency components in the profile of the polished surface across the direction of polish, mostly due to the ridges along the polish lines. The brightness of the specularly reflected spot is indicative of the high reflectance of the surface, and the smooth profile along the grooves of the surface. A typical micrograph of the unirradiated surface is also shown in figure 17a.

Figure 17b shows the scattering pattern from the centre of the irradiated zone of specimen S5 (150 W, 240 s). The optical micrograph of the corresponding surface shows distributed tiny pits indicating the initiation of melt. Though this is not apparent visually, nucleation of melt zones is clearly seen in the optical micrograph. There is coalescence between some of them to form connected clusters, though but complete melting is yet to take place. The nucleation of melt zones has resulted in proportional loss in the virgin surface (comprising emery tracks during polishing). Also the sharp edges of these grooves are smoothened at near melting temperatures. As a result there is decrease in the high spatial frequency components in the scattering pattern. Correspondingly, there is a decrease in the spread of the streak in the scattering pattern. An increase in the width of the specular reflected spot is also observed. This is attributed to decrease in the smooth surface along the grooves, which has been replaced by rippled molten surface.

In the specimens S-7 (200 W, 75 s) to S-9 (200 W, 120 s), the irradiated zone has completely melted to form a pit. The scattering from the pit is highly diffused, with drastic reduction

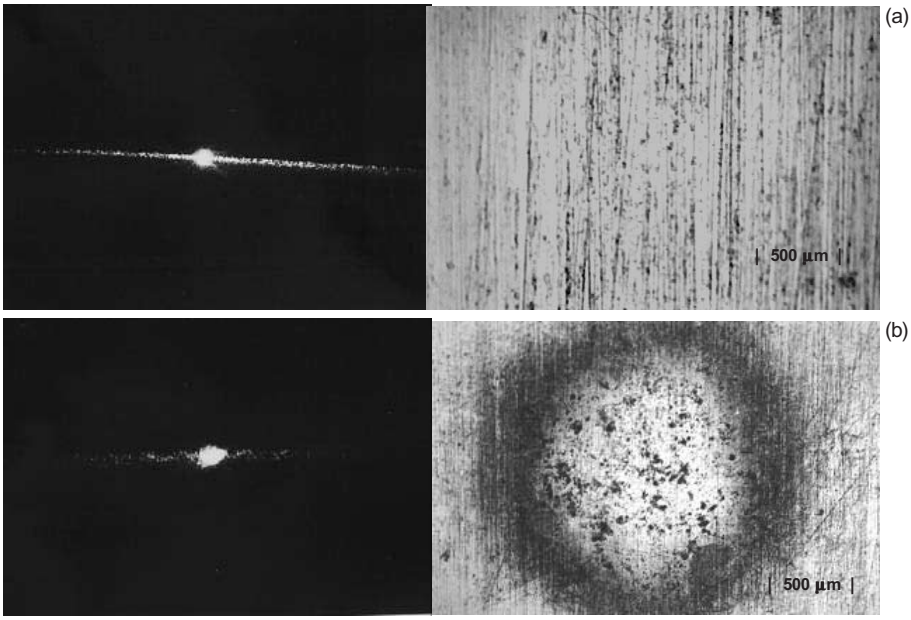

Figure 17. **(a)** Typical scattering pattern from unirradiated polished surface and micrograph of the surface of the unirradiated zone. **(b)** Scattering pattern from the centre of the irradiated zone (150 W, 240 s) and optical micrograph of the corresponding surface.

in the intensity, indicating steep profiled surface of the pit. Thus laser-scattering can clearly differentiate different stages of laser-induced surface modification.

The morphology of the scattering pattern appears to be a convenient measure to differentiate these stages. The shape factor of the scattering pattern is given by (perimeter^2/(4.π. area)), and is a measure of deviation from circularity. If the scattering is isotropic the shape factor is expected to be close to 1·0.

Figure 18 shows the shape factor as a function of visual classification. Clearly, there is a distinct almost non-overlapping clustering of shape factors depending upon the classification of the treated surface. Thus a correlation is established between the shape factors of the scattering pattern and the condition of the modified surface. The upper bounds of clusters corresponding to white-hot can be considered as limiting exposure factors to avoid surface melting. Thus 3·0 and 4·7 are the limiting measures of shape factor and aspect ratio respectively.

The reported measurements are off-line. That is, after they are removed from the laser irradiation platform. This introduces some surface modifications due to recovery of the surface, or solidification of the melt region etc. On-line measurements are feasible. However, the results would be different. But authors believe that feedback on the process is possible to ensure appropriate treatment, after due validating measurements. While studying laser-scattering behaviour of laser-irradiated specimens on-line, one should take appropriate measures to filter out wavelengths other than the probe wavelength. Also, precautions must be taken to protect the optical set from possible damage due to scattering or stray radiation of the high power laser beam. Apart from this, one has to consider air turbulance near the surface which affects the scattering pattern. Air turbulence may not be a problem if the laser heat treatment is being done in vacuum.

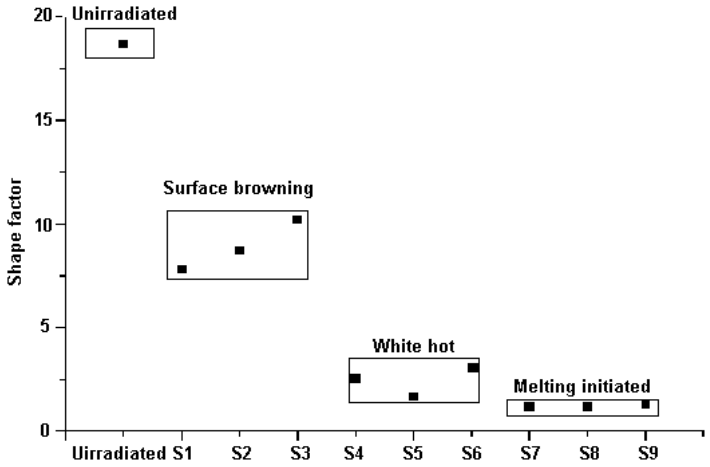

Figure 18. Shape factor of scattering pattern as a function of visual classification.

7. Conclusion

The possibility of using laser-scattering as a measure of surface roughness monitoring is described and discussed. A few case studies are presented. The need for careful choice of optical configuration and detailed calibration is evident from the description.

The authors thank Ms S Sosamma, Ms A V Anantha Lakshmi, Mr R V Subba Rao, Dr U Kamachi Mudali, Dr R Kesavamoorthy and Mr P Kalyanasundaram for their contribution to this work and Dr P Rodriguez, former Director, IGCAR for his encouragement and support.

References

Ananta Lakshmi A V, Djamouna P, Kamachi Mudali, Babu Rao C, Baldev Raj 1999 Study of corrosion pits using laser-scattering. *Optics and optoelectronics, theory, devices and applications* (eds) O P Nijhavan, A K Gupta, A K Musla, Kehar Singh (New Delhi: Narosa) vol. 1, pp 321–324

Beckmann P, Spizzichino A 1963 *The scattering of electromagnetic waves from rough surfaces* (Oxford: Pergamon)

Bennett H E 1978 Scattering characteristics of optical materials. *Opt. Eng.* 17: 480–488

Bennett J M 1992a Recent developments in surface roughness characterisation. *Meas. Sci. Technol.* 3: 1119–1127

Bennett J M 1992 *Surface finish and its measurement.* (Washington, DC: Opt. Soc. Am.)

Bennett J M, Dancy J H 1981 Stylus profiling instrument for measuring statistical properties of smooth optical surfaces. *Appl. Opt.* 20: 1785–1802

Bennett J M, Mattsson L 1989 *Introduction to surface roughness and scattering* (Washington, DC: Opt. Soc. Am.)

Brecker H N, Fromson R E, Shum L Y 1977 A capacitance-based surface texture measuring system. *Ann. CIRP.* 25 (1): 375–377

Bristow T C, Bouzid A, Bietry J 1988 Surface measurements and applications for manufactured parts using noncontact profilometry. Optical testing and metrology II (ed) C P Grover, *Proc. Soc. Photo-Opt. Instrum. Eng.* 954: 217–25

Cao L X, Vorburger T V, Lieberman A G, Lettieri T R 1991 Light scattering measurement of the rms slopes of rough surfaces. *Appl. Opt.* 30: 3221–3227

Chmiel J, Cieszczyk-Chmiel A, Matysik J 1990 The use of interferometry in corrosion investigation. *Corrosion.* 6: 234–250

Church E L 1979 The measurement of surface texture and topography by differential light scattering. *Wear* 57: 93–105

Clarke G N, Thomas T R 1979 Roughness measurement with a laser scanning analyser. *Wear* 57: 107–116

Escalona R, Deviflers R, Tribillon G 1993 Application of phase shifting interferential microscopy to pitting corrosion studies of ion-implanted stainless steel. *J. Mater. Sci.* 28: 999–1006

Feng J, Chiang F P 1997 A new technique using digital speckle correlation for nondestructive testing of corrosion. *Mater. Evaluation* 55: 813–816

Galerie A, Pons M, Caillet M 1987 Elaboration d'alliages de surface sous irradiation laser. *Meas. Sci. Technol.* 88: 127–134

Garatt J D 1979 Survey of displacement transducers below 50 mm. *J. Phys.* E12: 563–573

Graneck M, Wunsch H L 1952 Application of pneumatic gauging to the measurement of surface finish. *Machinery* 81: 701–707

Hingle H T, Rakels J H 1983 The practical application of diffraction techniques to assess surface finish of turned parts, *Ann. CIRP* 32 (1): 499–501

Lessor D L, Hartman J S, Gordon R L 1979 Quantitative surface topography determination by Nomarski reflection microscopy. 1. *Theory. J. Opt. Soc. Am.* 69: 57–66

Matthews H J, Hamilton D K, Sheppard C J R 1986 Surface profiling by phase-locked interferometry. *Appl. Opt.* 25: 2372–2374

Ogilvie S R, Isakov E, Glover P W J, Taylor C W 2001 A new high resolution optical method for obtaining the topography of fracture surfaces in rocks. *8th European Congress for Stereology & Image Analysis*, Bordeaux, France, Sept 4–7, pp 208–209

Pearce J T H 1997 Corrosion – a layman's guide. *Insight* 39: 10–16

Pelletier J M, Vannes A B, Pilloz M, Vincent L 1993 Laser surface treatments and mechanical properties. *Lasers Eng.* 1: 251–270

Pool R 1990 The children of the STM. *Science* 247: 634–636

Proc. SPIE 2000 vol.4100 1–2 August

Radhakrishnan V 1977 Application of inductive heads for non-contact measurement of surface finish. *Proc. Int. Conf. Prod. Eng. Calcutta*, pp 80–89

Radhakrishnan V, Sagar V 1970 Surface roughness assessment by means of pneumatic measurement. *Proc. AIMTDR Conf.*, Madras, pp 487–494

Rakels J H 1986b The use of Bessel functions to extend the range of optical diffraction techniques for in-process surface finish measurements of high precision turned parts. *J. Phys.* E19: 76–79

Rakels J H 1986a Diffraction, an old optical phenomenon, used as an advanced metrology tool, *Proc. Modern Production and Production Metrology* Vienna

Senthil Selvan J, Subramanian K, Nath A K 1999 Effect of laser surface hardening on En18 (AISI 5135) steel, *J. Mater. Proc. Technol.* 91: 29–36

Sheppard C J R, Matthews H J 1988 The extended-focus, auto-focus and surface-profiling techniques of confocal microscopy. *J. Modern Opt.* 35: 145–54

Sherrington I, Smith E H 1988 Modern measurement techniques in surface metrology: Part I: Stylus instruments, electron microscopy and non-optical comparators. *Wear* 125: 271–288

Sherwood K F, Crookall J R 1968 Surface finish assessment by an electrical capacitance technique. *Proc. Inst. Mech. Eng.* 182: 344–349

Stout K J 1984 Optical assessment of surface roughness. *Precis. Eng.* 6(1): 35–39

Tanner L H 1979 A pneumatic Wheatstone bridge for surface roughness measurement. *J. Phys. E* 12: 957–960

Thwaite E G 1980a Power spectra of rough surfaces obtained by optical Fourier transform. *Ann. CIRP.* 29(1): 419–422

Thwaite E G 1980b A quantitative comparision of the wavelength spectrum of a surface obtained by optical Fourier transform. *Ann. CIRP.* 29: 419–422

Vaidehi G, Vanmathy R, Babu Rao C, Baldev Raj 1995 Characterisation of the sodium exposed AISI type SS 316 surface using laser speckle pattern. Presented at course cum conference on lasers. Eurolaser Academy & Technical University of Vienna (Vienna: Euro Laser Academy)

Vorburger T V, Teague E C 1981 Optical techniques for on-line measurement of surface topography. *Precis. Eng.* 3: 61–83

Wagner J C 1967 Surface effects in pneumatic gauging. *Int. J. Mech. Tool. Des. Res.* 7: 1–14

Whitley J O, Kusy R P, Mayhew M J, Bucthal J E 1987 Surface roughness of stainless steel and electroformed nickel standards using a He–Ne laser. *Opt. Laser. Tech.* 19: 189–195

Wickramasinghe H K 1989 Scanned-probe microscopes. *Sci. Am.* 261: 98–105

Wilson T, Carlini A R, Hamilton D K 1986 Images of thick step objects in confocal scanning microscopes by axial scanning. *Optik* 73: 123–126